Journal of Ceramic Processing Research. Vol. 17, No. 10, pp. 1046~1051 (2016)

J O U R N A L O F
Ceramic Processing Research

Elastic wave characteristics from friction and wear of Si_3N_4 depending on the amount of SiO_2 nano-colloid

Seok-Hwan Ahn[a] and Ki-Woo Nam[b]

[a]*Dept. of Mechatronics, Jungwon University, Goesan-gun, Chungbuk 28024, South Korea*
[b]*Dept. of Materials Science and Engineering, Pukyong National University, 365 Sinseonro, Nam-gu, Busan 48547, South Korea*

Ceramics are highly useful materials as frictional materials, because of their high hardness and high heat resistance. This study analyzed the elastic wave characteristics in the abrasion test of two types of Si_3N_4. The friction coefficients of non-coated ceramics with SiO_2 nano-colloid were almost similar to that without. However, the friction coefficients of heat-treated ceramics with SiO_2 nano-colloid coating differed, varying with the amount of SiO_2 nano-colloid, and the heat treatment temperature. The characteristics of elastic waves generated during friction and wear were similar for the two types of ceramics. The results show that the mechanical properties, such as strength, are determined by the components of the main ceramics in sintering.

Key words: Friction and wear, Friction coefficient, Si_3N_4 ceramics, SiO_2 nano-colloid, Elastic wave.

Introduction

Ceramics are considered highly useful as frictional materials, because of their high hardness and high heat resistance. Silicon nitride, which is well known as a structural ceramic, with excellent mechanical properties [1-3], is a serious candidate for frictional materials. The wear properties of such a structural ceramic material have been extensively investigated, in different environments [3-8]. However, micro-cracks that develop during the machining process grow under operating conditions, and the safety of the structure is compromised.

In resolve this issue, many researchers addressed the use of Si_3N_4 monolithic [9-15], Si_3N_4/SiC composites [16-21], and ceramics [22-30] with SiO_2, to contribute to crack healing. Similarly, many studies are being conducted for friction, wear and crack-healing. But, research on the state of ceramics by analysis of the elastic wave detected from friction and wear conditions has not been conducted. Therefore, in this study, the acoustic wave generated during the wear test was detected for both types of specimens, and frequency analysis was carried out, according to the state of the specimen.

The first Si_3N_4 specimens were sintered with different amount of SiO_2 nano-colloid, which is known as a crack-healing material. The second specimens were coated with SiO_2 nano-colloid on a mirror polished surface, and were given heat treatment at 1273 K for 1 hr in air. After that, the specimens were given heat treatment for 10 min. at 1073, 1273, and 1573 K.

*Corresponding author:
Tel : +82-51-629-6358
Fax: +82-51-629-6353
E-mail: namkw@pknu.ac.kr

Experimental Method

A powder composed of 0.2 μm Si_3N_4, 0.27 μm SiC, and a sintering additive (33 nm Y_2O_3, commercially purchased anatase TiO_2, and 12% SiO_2 nano-colloid) was used for the experiments. The powder was composed of Si_3N_4 80 wt.% and SiC 20 wt.%. Y_2O_3 5 wt.% and TiO_2 3 wt.% were added to the powder, as sintering additives. To analyze the elastic wave characteristics effects based on the amount of SiO_2 nano-colloid employed, 0.0 wt.%, 1.3 wt.%, 2.6 wt.% and 10.4 wt.% of 12% SiO_2 nano-colloid were separately added as a sintering additive. The compositions of each specimen are show in Table 1. Alcohol and Si_3N_4 ball was added to this mixture, and blended completely for 24 hrs. The mixture was placed in a desiccator to extract the solvent, and to make a dry powder mixture. Circular plates of 60 × 5 mm were sintered in nitrogen gas for 1 hr, via a hot press under 35 MPa at 2123 K.

First, the specimens were cut into rectangular (3 × 4 × 10 mm^3) bars, and polished. Second, heat treatment was conducted, after coating the SiO_2 nano-colloid on the polished surface under 1273 K, for 1 hr in air. To analyze the effect of the heat treatment at high

Table 1. Batch composition of specimens.

	Si_3N_4 (wt.%)	SiC (wt.%)	Y_2O_3 (PHR)	TiO_2 (PHR)	SiO_2 colloid (PHR)
SSTS-1	80	20	5.0	3.0	0.0
SSTS-2					1.3
SSTS-3					2.6
SSTS-4					10.4

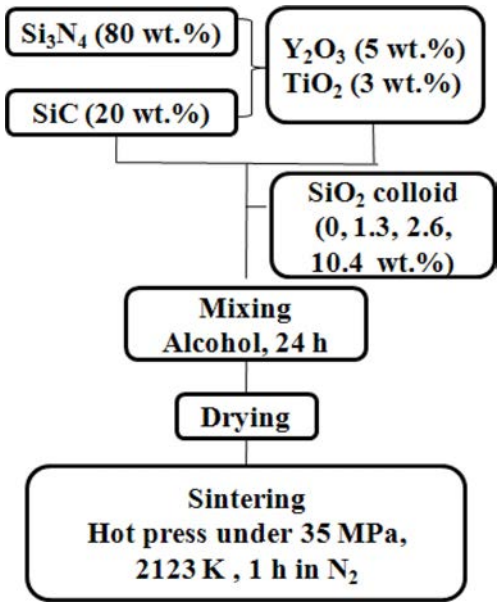

Fig. 1. Sintering flow chart.

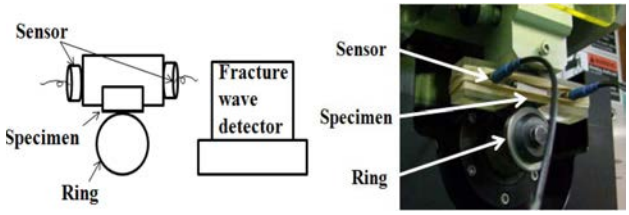

Fig. 2. (a) Schematic diagram and (b) actual appearance of elastic wave measurement system.

temperature, specimens were given heat treatment for 10 minutes, under three temperatures, 1073, 1273 and 1573 K. The tests were carried out 5 times, for each condition. Fig. 1 shows the sintering flow chart of Si_3N_4 ceramics.

The ring against wear specimen was QT vacuum heat treated SKD11, with diameter of 35 mm, and thickness of 7 mm.

The method used for testing in this study was the block on ring method (BRW140, NeoPlus). The fixed ring is rotating, and the loaded specimen and the ring are in face-to-face contact. The total wear time was 5,500 second, at normal temperature, and dry state. Because the lever ratio was 5 : 1, the tester load was 9.8 N, using a weight of 1.96 N. The rotational speed of the ring was 50 rpm. In addition, the surface roughness was measured using the Mitutoyo Surftest (SJ-301), in order to examine the effect of the surface condition on elastic waves.

Figs. 2(a) and 2(b) are a system schematic, and photographs of the fracture wave detector (FWD, FM-1, Digital Wave Corp., Englewood Co.) used to obtain the elastic wave signal, respectively. The jig of the elastic wave detection sensor was made using a plastic plate, and the sensor was fixed with a rubber band in the test piece. In this experiment, the duration time of an event was about 102.4 ìsec. Elastic wave signals were subjected to frequency analysis, using wavelet analysis.

Wavelet Analysis Method

The mean-square wavelet maps used in this study are briefly described [19]. A function is used to measure waveforms or arbitrary waveforms. This function can be expressed by the following equation.

$$f(x)=a_0+\sum_j\sum_k a_{2^{j+k}}W(2^jx-k)\ 0\le x\le 1 \tag{1}$$

Here, a is the wavelet coefficient, and $W(2^jx-k)$ is the wavelet function. This function has a square waveform, which is integrated from the start (0), to the end (1) of the signal.

$$\int_0^1 f^2(x)dx=a^2{}_o+2a_o\sum_j\sum_k a_{2^{j+k}}\int_0^1 W(2^jx-k)dx+\cdots$$

$$+\sum_j\sum_k\sum_r\sum_s a_{2^{j+k}}a_{2^{r+s}}\int_0^1 W(2^jx-k)W(2^rx-s)dx \tag{2}$$

The orthogonality and the area characteristics of the wavelet function become square terms for the coefficients of the wavelet function. Then, the square terms of each coefficient are represented by the horizontal axis (time), and the longitudinal axis [19].

$$\int_0^1 f^2(x)dx=a_0{}^2+a_1{}^2+\frac{1}{2}(a_2{}^2+a_3{}^2)+\frac{1}{4}(a_4{}^2+\cdots+a_7{}^2)$$
$$+\frac{1}{8}(a_8{}^2+a_9{}^2+\cdots+a_{15}{}^2)+\frac{1}{16}(a_{16}{}^2+\cdots+a_{31}{}^2) \tag{3}$$

That is, the square terms of the wavelet coefficients for the function are represented by a log scale on the longitudinal axis. This is exponentially shortened, and the frequency is increased in multiples. The wavelet amplitude shows the density distribution of the frequency spectra as a type of contour line. The relationship of time-frequency is display as a contour. Typical contour lines are shown in Fig. 9(c).

Results and Discussion

Surface roughness

Fig. 3 shows the following cases of roughness: (a) the grinding surface by ring of SKD11, (b) the mirror-polished surface of SSTS-1, and (c) the heat treated surface at high temperature with the SiO_2 nano-colloid coating, on the mirror-polished surface of SSTS-1. (a) shows a roughness of less than 0.5 μm, while (b) partially shows a large roughness by polishing. But, even though (c) shows micro roughness by heat treatment with SiO_2 nano-colloid coating, the roughness, which indicates a large value by polishing, is not lost by heat treatment by SiO_2 nano-colloid coating, and remains. The arithmetic

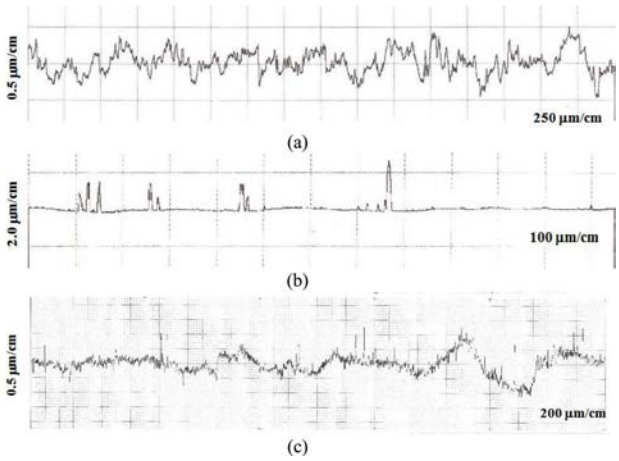

Fig. 3. Surface roughness of Si_3N_4 with heat treatment in high temperature; (a) SKD-11, (b) SSTS-1, (c) SSTS-1 (1273 K).

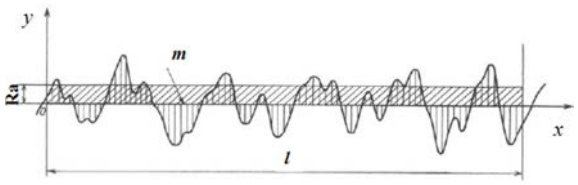

Fig. 4. Evaluation method of Ra.

mean roughness (Ra) values are summarized in Table 2.

In the roughness curve, the x-axis is the measured length, and the y-axis is the roughness scale. When the roughness curve is represented as y = f(x), Ra is shown in ß¦, a value obtained by the following equation;

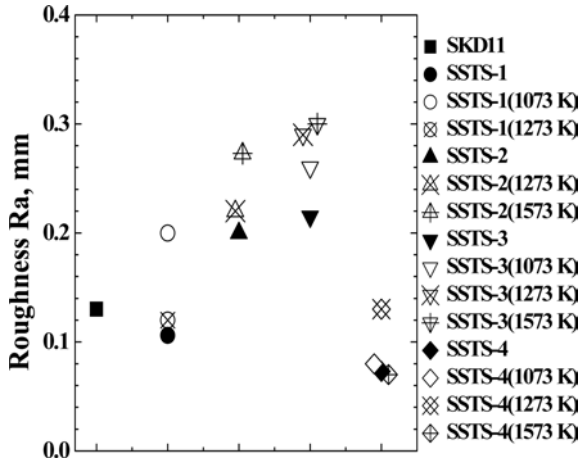

Fig. 5. Roughness depending on coating of SiO_2 colloid.

$$R_a = \frac{1}{l}\int_0^1 |f(x)|dx \tag{4}$$

Here, l is a reference length. Fig. 4 shows how to obtain Ra.

Fig. 5 shows the surface roughness for each condition of Table 2. The surface roughness of SKD11 was approximately 0.13 μm. The roughness of mirror-polished ceramic specimens (● , ▲ , ▼ , ◆) differed, depending on the accuracy of polishing. Meanwhile, in the case of SiO_2 nano-colloid coating on a mirror-polished surface, the roughness of the heat-treated ceramics specimen was slightly larger, than that of the mirror-polished specimen. This is a result of SiO_2 nano-sized particles being formed on the surface during heat-treatment.

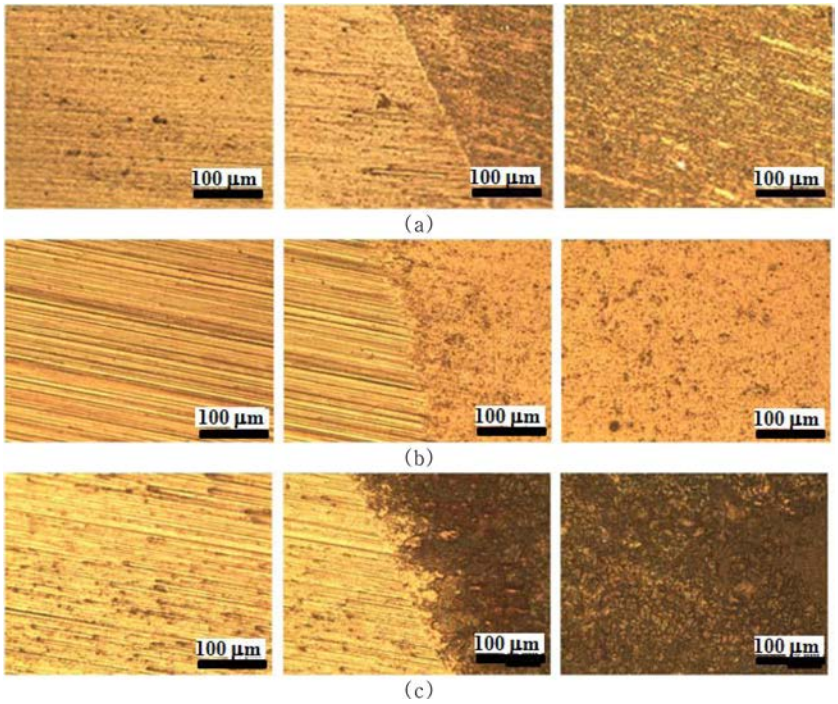

Fig. 6. Optical microscope image of wear part, boundary part and base part; (a) SSTS-1, (b) SSTS-1 (1073 K), (c) SSTS-2 (1573 K).

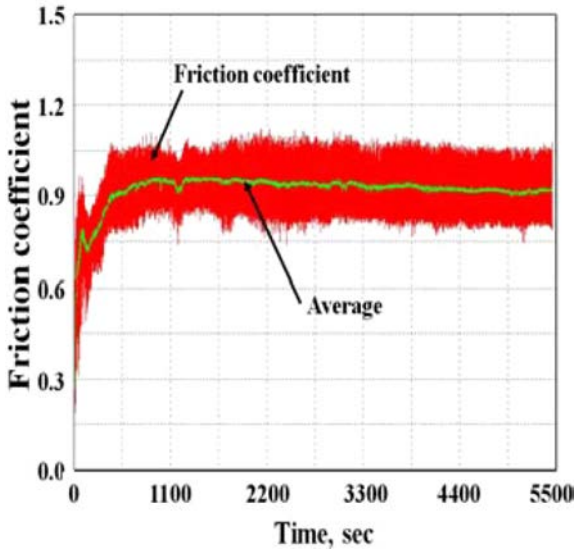

Fig. 7. Friction coefficient from SSTS-4 (1273 K).

Table 2. Surface roughness for each specimen.

	Ra (μm)	Remarks
SKD11	0.130	Ring
SSTS-1	0.106	Polished specimens
SSTS-2	0.200	
SSTS-3	0.215	
SSTS-4	0.073	
SSTS-1 (1073 K)	0.200	Heat treatment after coating of SiO_2 colloid on polished specimens
SSTS-1 (1273 K)	0.120	
SSTS-2 (1273 K)	0.220	
SSTS-2 (1573 K)	0.273	
SSTS-3 (1073 K)	0.260	
SSTS-3 (1273 K)	0.290	
SSTS-3 (1573 K)	0.300	
SSTS-4 (1073 K)	0.080	
SSTS-4 (1273 K)	0.130	
SSTS-4 (1573 K)	0.070	

Wear behavior

A representative optical micrographs after the wear test is shown in Fig. 6. It was difficult to identify the wear part from the ring, but the wear part, the boundary part and the base part were clearly distinguished for the Si_3N_4 specimens. In the figure, the wear part is observed as a scratched or a striped shape, compared to the base part. This is the behavior of abrasive wear. Abrasive wear is responsible for 50% of loss caused by wear. This is the main mechanism in the deformation by micro shear. The Si_3N_4 specimens showed different surface color, according to the heat treatment temperature. This indicates the degree of oxidized surface, according to the heat treatment temperature. There was not a clear correlation between degree of oxidation, and roughness.

Fig. 7 shows SSTS-4 (1273 K), which is a typical example of the relation between the friction coefficient, and the time obtained during the wear test. The x-axis represents the wear distance, while the y-axis represents the coefficient of friction. The friction coefficient increases in a curve until about 550 second, and then remains constant. The constant region was defined as the friction coefficient. Table 3 is an average value of the friction coefficients measured in the experiments.

Table 3. Average friction coefficient for each specimen.

	Average friction coefficient	Remarks
SSTS-1	0.900	Polished specimen
SSTS-2	0.790	
SSTS-3	0.808	
SSTS-4	0.850	
SSTS-1 (1073 K)	0.470	Heat treatment after coating of SiO_2 colloid on polished specimens
SSTS-1 (1273 K)	0.625	
SSTS-2 (1273 K)	0.720	
SSTS-2 (1573 K)	0.530	
SSTS-3 (1073 K)	0.820	
SSTS-3 (1273 K)	0.920	
SSTS-3 (1573 K)	1.030	
SSTS-4 (1073 K)	0.750	
SSTS-4 (1273 K)	0.920	
SSTS-4 (1573 K)	0.900	

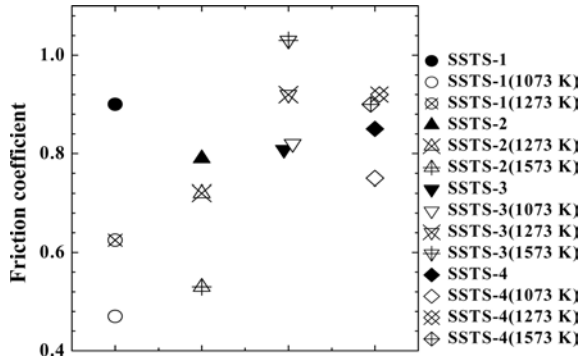

Fig. 8. Friction coefficient depending on coating of SiO_2 colloid.

Fig. 8 shows friction coefficient depending on coating of SiO_2 colloid. The friction coefficients for the four kinds of specimen of SiO_2 colloid non-coating were almost similar. But the solid circle (●) without SiO_2 colloid addition, appeared slightly larger than the solid triangle (▲), the solid inverted triangle (▼), and the solid rhombus (◆), with SiO_2 colloid addition. However, heat-treated specimens by SiO_2 colloid coating yielded different friction coefficients, in accordance with the amount of addition of SiO_2 colloid, and the heat treatment temperature. By the heat treatment with SiO_2 colloid coating, a small friction coefficient was shown by SSTS-1 without SiO_2 colloid, and SSTS-2 with 1.3 PHR of SiO_2 colloid. But SSTS-3 and SSTS-4, with 2.6 and 10.4 PHR of SiO_2 colloid, respectively, showed significant friction. In addition, heat-treated specimens, rather than uncoated specimens, showed a small friction

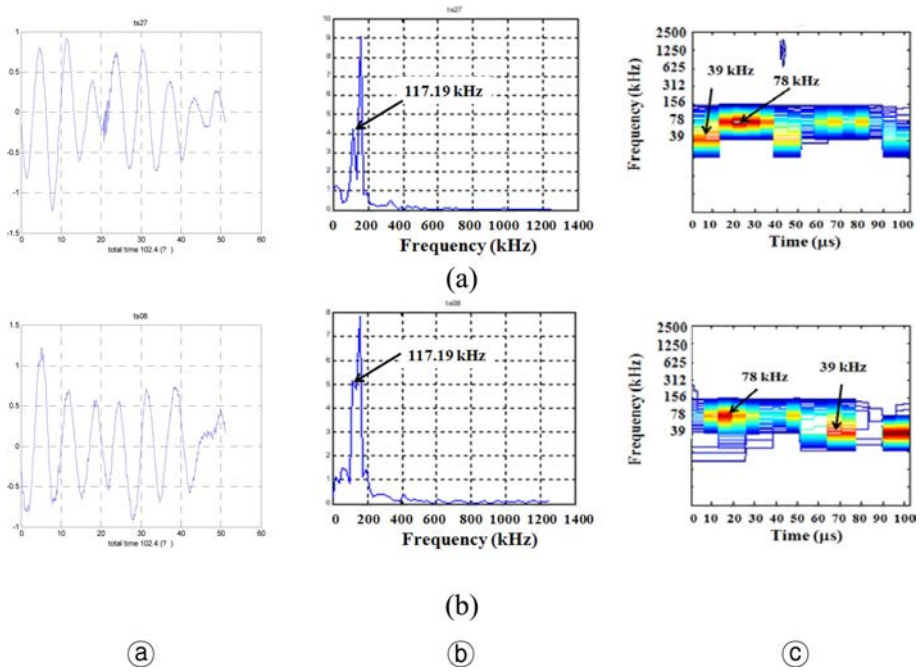

Fig. 9. ⓐ Time response of elastic wave signal, ⓑ Frequency spectrum and ⓒ Contour map of wavelet analysis; (a) SSTS-1, (b) SSTS-1 (1073 K)

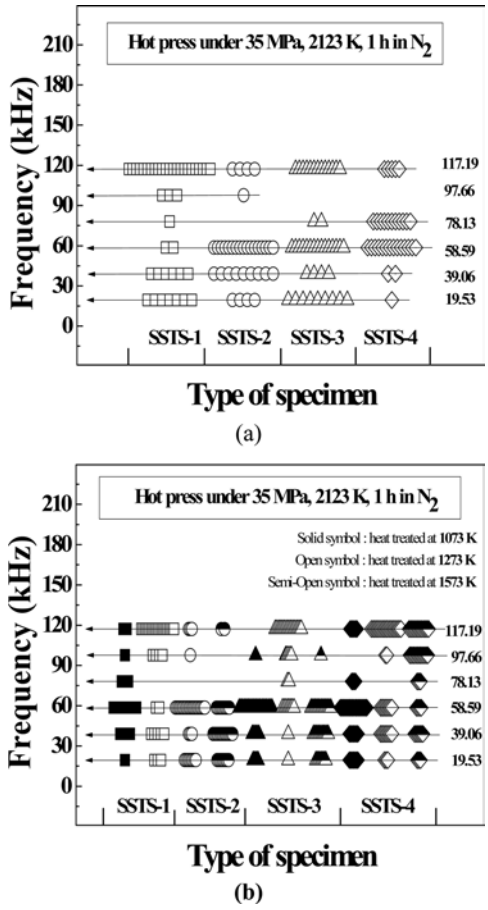

Fig. 10. Dominant frequencies from (a) SSTS-1 and (b) SSTS-1 (1073 K).

coefficient at 1073 K, and showed significant friction at 1273 and 1573 K, respectively. It is concluded that the coating layer and SiO_2 on the surface by heat treatment will result in even more hardening.

Characteristics of elastic wave

The elastic waves of sintered Si_3N_4 with differing amounts of addition of SiO_2 nano-colloid, i.e. non-coating Si_3N_4 of SiO_2 nano-colloid, and heat-treated Si3N4 for 10 minutes at high temperature by coating with SiO_2 nano-colloid, were detected during the wear test. The signals were subjected to frequency analysis, according to the type of specimen. Representative results are shown in Fig. 9. Fig. 9(a) shows the wavelet analysis results of the elastic wave ⓐ, the spectral density © of the highest frequency, which was around 78 kHz, and which was 117.19 kHz in frequency analysis ⓑ. The frequency of 117.19 kHz was displayed at 78 kHz, of the vertical axis of ⓒ. As described in the wavelet analysis, the reason is that the middle value of each level appears on the vertical axis. That is, all components from 19.53 kHz to 117.19 kHz of the frequency spectrum density are presented in the form of contour lines that appear centered on 78 kHz. The frequency of 117.19 kHz of ⓑ shows the highest dominant frequency components, by the arrows in the spectral density of ⓒ. In many cases, these frequency components are included in the initial generation of the burst type signal. Fig. 9(b) displays a similar dominant frequency, to that shown in Fig. 9(a). Therefore, it is considered that the mechanical properties, such as strength, are decided by the components of the main ceramics in sintering.

Fig. 10(a) shows the dominant frequency band of a non-coated specimen of SiO_2 nano-colloid. All of these signals would be obtained by abrasion. SSTS-1 represents the dominant frequency of 117.19 kHz, and

also shows a dominant frequency below 39.06 kHz. SSTS-2, SSTS-3, and SSTS-4 with SiO_2 nano-colloid display a dominant frequency of 117.19 kHz, and also show a dominant frequency of 58.59 kHz. The dominant frequency of 39.06 kHz decreases, and that of 78.13 kHz appears, according to increases of the amount of SiO_2 nano-colloid. Thus, it is determined that the dominant frequency of SSTS-1 is 117.19 kHz; while the dominant frequencies of both SSTS-2 and SSTS-3 are 117.19 kHz and below 58.59 kHz, and of SSTS-4 are 78.13 kHz and 58.59 kHz. Fig. 10(b) shows the dominant frequency band of the heat-treated Si_3N_4 for 10 minutes at high temperature, by coating with SiO_2 nano-colloid. In this figure, high dominant frequencies are detected, as the amount of SiO_2 nano-colloid and the heat treatment temperature increase. But overall, the dominant frequency shows a similar trend to that in (a).

Conclusions

This study was to detect and analyze the elastic wave characteristics, in the abrasion test of two types of Si_3N_4. The results were as follows:

1) The roughness of mirror-polished ceramics varied, depending on the precision of polishing. The roughness of heat-treated ceramics with SiO_2 nano-colloid coating was slightly larger, than that of the non-coated specimens. The coating film formed on the surface and the nanoscale SiO_2 particles are caused by the heat treatment with SiO_2 nano colloid coating.

2) The friction coefficient of non-coated ceramics with SiO_2 nano-colloid showed almost similar. However, the heat-treated ceramics with SiO_2 nano-colloid coating differed, according to the amount of SiO_2 nano-colloid, and the heat treatment temperature.

3) The characteristics of the elastic waves generated during friction and wear of the two types of ceramics were similar. It is concluded that the mechanical properties, such as strength, are determined by the components of the main ceramics in sintering.

"This work was supported by the Jungwon University Research Grant(2015-020)".

References

1. R.N. Katz, Nitrogen ceramics, in: F.L. Riley (Ed.), Progress in Nitrogen Ceramics, Martinus Nijhoff Publishers, The Hague, The Netherlands, (1983) 3.
2. K.H. Jack, Sialons: a study in materials development in: S. Hampsshire (Ed.), Non-Oxide Technical and Engineering Ceramics, Elsevier Applied Science Publishers, New York (1986) 1.
3. M.J. Hoffmann, G. Petzow, Microstructure design of Si_3N_4 based ceramics, in: I.W. Chen, P.F. Becher, M. Mitomo, G. Petzow, T.S. Yen (Eds.), Silicon Nitride Ceramics, Material Research Society, Pittsburgh, PA (1993) 3.
4. S.S. Kim, Y.H. Chae, D.J. Kim, Tribology Letters 9 (2000) 227.
5. C.P. Dogan, J.A. Hawk, Wear 250 (2001) 256.
6. S.M. Hsu, M. Shen, Wear 256 (2004) 867.
7. M. Belmonte, P. Miranzo, M.I. Osendi, J.R. Gomes, Wear 266 (2009) 6.
8. H. Miyazaki, H. Hyuga, Y. Yoshizawa, K. Hirao, T. Ohji, J. of the European Ceramic Society 29 (2009) 1535.
9. M. Mitomo, T. Nishimura and M. Tsutsumi, J. Mater. Sci. Lett. 15 (1996) 1976.
10. Y.Z. Zhang, L. Edwards and W.J. Plumbridge, J. Am. Ceram. Soc. 81 (1998) 1861.
11. K. Houjou, K. Ando, S.P. Liu and S. Sato, J. Eur. Ceram. Soc. 24 (2004) 2329.
12. K. Ando, M.C. Chu, Y. Kobayashi, F. Yao and S. Sato, JSME 65 (1999) 1132.
13. S.K. Lee, W. Ishida, S.Y. Lee, K.W. Nam and K. Ando, J. Eur. Ceram. Soc. 25 (2005) 569.
14. K.W. Nam, S.W. Park, J.Y. Do and S.H. Ahn, Transactions of the Transactions of the KSME A32 (2008) 957.
15. K.W. Nam, S.H. Park, K.K. Eun and J.S. Kim, Transactions of the KSME A34 (2010) 1715.
16. K. Ando, T. Ikeda, S. Sato, F. Yao and Y. Kobayashi, Fatigue Fract. Eng. Mater. Struct. 21 (1998) 119.
17. K. Ando, K. Houjyou, M.C. Chu, S. Takeshita, K. Takahashi, S. Sakamoto and S. Sato, J. Eur. Ceram. Soc. 22 (2002) 1339.
18. K. Ando, K. Takahashi, S. Nakayama and S. Saito, J. Am. Ceram. Soc. 85 (2002) 2268.
19. K.W. Nam, M.K. Kim, H.S. Kim, J.W. Kim and S.H. Ahn, International Journal of Modern Physics B20 (2006) 4279.
20. M.K. Kim, S.W. Park, C.S. Son, S.H. Ahn and K.W. Nam, Proceeding of The KSME 2006 Fall Annual Meeting (2006) 149.
21. K.W. Nam, M.K. Kim, S.W. Park, S.H. Ahn and J.S. Kim, Materials Science and Engineering A471 (2007) 102.
22. M.K. Kim, S.B. Kang, S.H. Ahn and K.W. Nam, Solid State Phenomena 124 (2007) 719.
23. S.W. Park, M.K. Kim, S.H. Ahn and K.W. Nam, 2006 Annual Conference & International Workshops of the 20th Anniversary of the Korean Society of Ocean Engineers (2006) 166.
24. K.W. Nam, M.K. Kim, S.W. Park, S.H. Ahn and J.S. Kim, Materials Science and Engineering A471 (2007) 102.
25. K.W. Nam, J.S. Kim and H.B. Lee, Transactions of the KSME A33 (2009) 652.
26. K.W. Nam, S.H. Park and J.S. Kim, Journal of Ceramic Processing Research 10 (2009) 497.
27. K.W. Nam and K.C. Lee, Transactions of the KSME A33 (2009) 1233.
28. K.W. Nam and J.S. Kim, Journal of Ceramic Processing Research 11 (2010) 20.
29. K.W. Nam, J. S. Kim & S. W. Park, International Journal of Modern Physics B24 (2010) 2869.
30. K.W. Nam, J.S. Kim and S.W. Park, Materials Science and Engineering A527 (2010) 5400.